Materials Advances

ROYAL SOCIETY OF CHEMISTRY

PAPER

View Article Online
View Journal | View Issue

Cite this: *Mater. Adv.*, 2025, **6**, 8011

Sustainable synthesis of Nd_2O_3 nanoparticles for photocatalytic degradation of tetracycline in aqueous media

Sadia Muzammal,†[a] Awais Ahmad, †*[bf] Sadia Atta,[c] Afzal Hussain,[d] Shafaqat Ali,*[ae] Ayesha Sadiqa*[b] and Patrizia Bocchetta*[f]

Received 9th June 2025,
Accepted 20th July 2025

DOI: 10.1039/d5ma00615e

rsc.li/materials-advances

The great discrepancy in crystal size and incongruity in the crystal interface of catalysts lead to decreased catalytic performance, limiting their application for antibiotic removal. Herein, a regulation strategy *via* intrinsic ion interpenetration is proposed to engineer nanostructured Nd_2O_3 photocatalyst for efficient photocatalytic degradation of tetracycline (TC). Mechanism studies indicate that Nd_2O_3 NPs reduce metal ions into their elemental form, enabling oxygen atoms to adhere to the metal surfaces. Moreover, the degradation and mineralization rate of TC increased by 92% within 40 minutes by following first-order kinetics. Combining photocatalytic degradation with a first-order kinetics reaction could produce the oxygen-reactive species, which helps to enhance the degradation and mineralization rates of TC pollutants. Furthermore, the antibacterial efficiency of the as-synthesized Nd_2O_3 NPs was assessed against *Staphylococcus aureus* and *Escherichia coli*. This work presents a synergistic effect of Nd_2O_3 NPs in water purification and biomedical applications.

1. Introduction

The massive rise in global population raises the high demand for goods derived from agriculture and, at the same time, increases the global need for fresh water. Dyes, antibiotics, organic pollutants, pigments, pesticides, insecticides, and crop-based medicines also escalate the demand for fresh water. Pesticides and fungicides applied to crops during intense rainfall are immediately released into freshwater ponds, lakes, and rivers.[1,2] The excess amount of antibiotics and their penetration into the water bodies provide a highly toxic environment. It takes billions of years to degrade and remove this contamination from these water basins.[3] Tetracycline (TC), a widely used antibiotic, is another contaminant that has become an environmental concern due to its persistent nature. Serious drawbacks in water bodies remain due to their occurrence, which has led to emerging antibiotic-resistant bacteria, potentially harmful to aquatic systems. The erroneous disposal and persistence of antibiotics like TC have led to a boom in antibiotic resistance in marine environments and paved the way for rising global health concerns. The presence of TC and other antibiotics poses a serious threat to environmental and human health.[4–6] The breakdown of these substances takes a long time, and great efforts are required to remove them, in terms of time, energy, and resources, stressing the need for effective and eternal solutions. Bacterial resistance to TC makes it difficult or impossible to treat against antibiotic-resistant bacteria.[7] Agricultural runoff is another serious threat resulting from the improper disposal of TC, worsening this problem. The entire health system of humans was found to be at increased risk due to the intake of water or food contaminated with antibiotic-resistant bacteria that were resistant to standard treatments, increasing the burden on healthcare costs and systems.[8]

Various techniques, such as advanced and chemical oxidation, adsorption, photocatalysis, coagulation, and filtration, are available for organic pollutants. Among these, photocatalysis is the most promising approach using a catalyst, breaking down the pollutants into less harmful substances.[9,10] While various organic pollutants have been substituted for photocatalytic degradation, negligible work has been done on the photocatalytic degradation of TC. Among rare earth metal oxides, neodymium oxide (Nd_2O_3) has recently attracted enormous interest due to its wonderful properties, such as high thermal stability, high value, and band

[a] *Department of Environmental Sciences, Government College University, 38000, Faisalabad, Pakistan. E-mail: shafaqataligill@yahoo.com*
[b] *Department of Chemistry, The University of Lahore, Lahore, Pakistan. E-mail: awais.ahmad@chem.uol.edu.pk, ayesha.sadiqa@chem.uol.edu.pk*
[c] *Department of Chemistry, University of Punjab, Lahore, Pakistan*
[d] *Department of Environmental Sciences, The University of Lahore, Lahore, Pakistan*
[e] *Department of Biological Sciences and Technology, China Medical University, Taichung 40402, Taiwan*
[f] *Department of Innovation Engineering, University of Salento, 73100, Lecce, Italy. E-mail: patrizia.bocchetta@unisalento.it*
† Sadia Muzammal and Awais Ahmad contributed equally as first authors.

gap energy of approximately 4.6 eV.[11] It has wide applications in catalysts, UV absorbents, luminescent materials, pro-coatings, and magnets.

Sol–gel, hydrogen plasma-metal reaction, precipitation, thermal breakdown, CVD, sputtering, green synthesis, and thermal combustion are a few ways to synthesize Nd_2O_3 nanoparticles (NPs).[12–15] Some of these methods involve the emission of harmful byproducts and are costly, time-consuming, and subject to particle aggregations. Green synthesis has been regarded as a significant method for metal oxide NPs due to the use of fewer chemicals. It is known that very few metal oxide NPs (CuO, ZnO, TiO_2, NiO, Co_3O_4, and Fe_2O_3) are synthesized using green methods with a variety of plant extracts and have also unveiled their antibacterial efficacy against various bacterial cultures.[16–18] *Caryota urens (C. urens)*, also known as fishtail palms, attract distinct interest in nanotechnology and biomedical sciences. This tropical plant has a rich phytochemical composition and is an eternal source of several bioactive compounds, such as flavonoids, steroidal saponins, tannins, polysaccharides, and phenolic acids.[19] These substances have diverse biological behaviors, such as antioxidant, anti-inflammatory, and antimicrobial properties.[19,20] A friendly alternative to conventional chemical methods is plant extract nanoparticle biosynthesis *via* green chemistry, which leverages the bioactive compounds in plants to enhance the stability and functionality of the synthesized nanostructures.[21] Specifically, zero-valent metal NPs were successfully biosynthesized using *Jasminum grandiflorum*, and unique properties obtained *via* the encapsulation of the plant's elements, facilitating the electron distribution in the interface of silicon and oxygen atoms.[22] The metal NPs *via* bioactive compounds in *C. urens* can play a crucial role as reducing agents and stabilizers, resulting in enhanced properties. Steroidal saponins were responsible for the stable and biocompatible coating over the NPs and served as capping agents. The uniformity and durability of the nanostructures were attained with flavonoids and phenolic acids, which further contribute to the reduction and stabilization processes.[23] A unique bio-organic interface resulting from the interaction between the metal NPs and the bioactive compounds in *Caryota urens* facilitates electron distribution between the metal atoms and lattice oxygen, stability, and functionality, making them suitable for diverse applications, particularly in biomedical and catalytic fields.[24] The novel aspect of this research lies in the fabrication of Nd_2O_3 NPs that have been utilized for the efficient environmental contaminant degradation of TC. Herein, the synthesized Nd_2O_3 NPs were subjected to substantial testing against *Staphylococcus aureus* and *Escherichia coli*. The Nd_2O_3 NPs using *C. urens* are unprecedented and represent a sustainable and eco-friendly method. The current focus of this study is to unveil the environmentally friendly biosynthesis procedure of *Caryota urens* extracts for the degradation of TC. The efficacy evaluation and the combat ability of Nd_2O_3 NPs against *Staphylococcus aureus* and *Escherichia coli* were investigated. The effectiveness of various photocatalysts and the reaction conditions were sufficient for efficient development of TC degradation and mitigated its environmental impact. This research emphasizes the development of nanotechnology and highlights the importance of sustainable practices in scientific innovation.

2. Materials and methods

2.1. Reagents

Neodymium(III) nitrate hexahydrate ($Nd(NO_3)_3{\cdot}6H_2O$, 99.9% AR-purity) and tetracycline ($C_{22}H_{24}N_2O_8$, 99.9% AR-purity) were purchased from Sigma Aldrich. These chemicals were prepared using double-distilled water, with no additional substances involved in the synthesis process.

2.2. Phytochemicals extraction

The leaf extract of *Caryota urens* was chosen as a reducer or stabilizer in the synthesis of Nd_2O_3 NPs. Initially, the collected *C. urens* leaves were weighed at 10 g and washed with double-distilled water to eliminate impurities. Following this, double-distilled water was used to wash the leaf thoroughly. Then the leaves were cut into tiny pieces and added to a beaker containing 100 mL of deionized water. The solution was boiled for 15 min at 70 °C using a heating mantle. After incubation, the filtrate was collected by the filtration process with Whatman No. 1® filter paper and stored in a brown bottle for further production of Nd_2O_3 NPs.

2.3. Green-mediated Nd_2O_3 NPs

The neodymium nitrate salt (0.0487 g) was dissolved in 90 mL of double-distilled water and placed on a hot plate for stirring. The plant leaf extract, 10 mL, was mixed into the neodymium nitrate solution, and the suspension was stirred at temperature of 70 °C. The appearance of a greyish-dark blue color denotes the formation of Nd_2O_3 NPs in the suspension. Furthermore, suspension was centrifuged at 8000 rpm for 8 min, and after that, the supernatant was removed, pellet was resuspended, and centrifugation was repeated 10 times (Fig. 1).

2.4. Characterization of Nd_2O_3 NPs

The crystalline structure and material stability were assessed using an X-ray diffractometer (PANalytical X'Pert) with Cu Kα radiation (1.5405 Å) at 30 kV and 40 mA. Optical properties were examined *via* UV-DRS (UV-2600 Shimadzu). FTIR spectroscopy (PerkinElmer) was employed to identify the functional groups of the Nd_2O_3 NPs and plant extract, covering a range from 4000 cm^{-1} to 400 cm^{-1}. Surface morphology and material composition were analyzed using FESEM (Carl Zeiss) and TEM (Titan) with EDX spectroscopy. The valence states and binding energies were investigated through X-ray photoelectron spectroscopy (XPS, PHI 5000 Versa Probe III, Physical Electronics, USA).

2.5. Experimental design, photocatalytic tests, and kinetics

The prepared Nd_2O_3 NPs were allowed to react with TC to confirm the degradation of antibiotics. Nd_2O_3 NPs (0.01 g) were mixed with 10 mg of 100 mL TC solution for degradation. The absorbance was recorded in 30-minute intervals and UV-vis spectroscopy of the reaction mixture (Nd_2O_3 NPs + TC) determined the degradation activity. The percentage of TC degradation is as

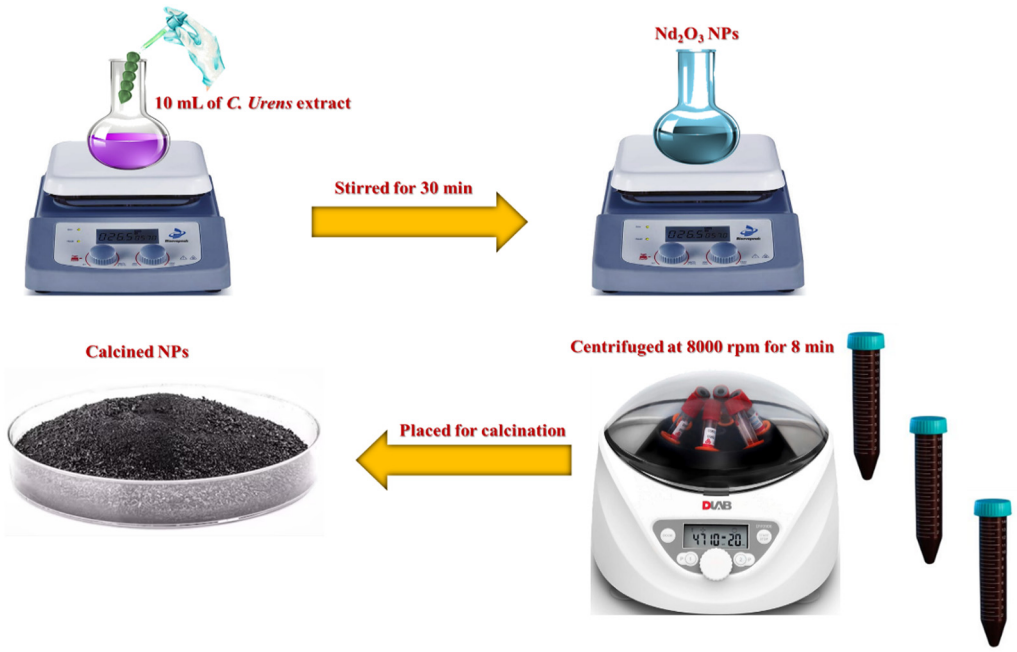

Fig. 1 Schematic illustration of the green-mediated formation of Nd_2O_3 NPs using an extract from *C. urens* leaves.

follows,

$$\text{Photocatalytic degradation} = \frac{C_0 - C_t}{C_0} \times 100 \quad (1)$$

$$r_p = -\frac{dC_p}{dt} = K_n C_p^n \quad (2)$$

In eqn (2), n is denoted as the reaction order found in a range of $0 \leq n \leq 2$.[25]

For $n = 2$. The integral form of eqn (2) is also known as a pseudo-first-order kinetic model and is expressed as follows:

$$C_p = C_{p,0} \exp(-K_1 t) \quad (3)$$

K_1 is known as the first-order rate constant. Eqn (3) can be rewritten as

$$\text{In}\frac{C_p}{C_{p,0}} = -K_1 t \quad (4)$$

In eqn (4), the $K_1 t$ value is denoted as the slope of a straight line of $\text{In}\frac{C_p}{C_{p,0}}$ *vs.* t.

2.6. Antibacterial efficacy of Nd_2O_3 NPs

The bacterial cultures of *S. aureus* (MTCC-902) and *E. coli* (MTCC-443) were procured from the Microbial Type Culture Collection (MTCC), Pakistan. Initially, a single bacterial culture of *S. aureus* and *E. coli* was inoculated into 100 mL of nutrient broth and incubated for 24 hours at 37 °C in a shaker. After 24 hours of incubation, bacterial cultures were separately swabbed on Muller–Hinton agar plates. Wells were made on the MHA plates using the gel puncture, and different concentrations of Nd_2O_3 NPs (10, 20, 50, and 100 μg mL^{-1}) were poured into the wells, and the plates were incubated for 24 h at 37 °C. The antibacterial efficacy of Nd_2O_3 NPs was confirmed by measuring the zone of inhibition formed around well after the incubation period (24 hours). A streptomycin antibiotic disc was used as a control for this antibacterial study.

3. Results and discussion

3.1. XRD analysis

The X-ray diffraction (XRD) analysis of bio-produced Nd_2O_3 NPs, as shown in Fig. 2, reveals a distinctive hexagonal crystalline structure with pronounced peaks at the 27.7° (100), 28.7° (002), 32.1° (101), 40.4° (102), 49.7° (110), 56.9° (103), 59.7° (112), 65.4° (004), 71.6° (203), and 78.7° (211) planes. The pronounced peaks were matched to the JCPDS card number 43-1023, thus signifying the authenticity and credibility of the bio-produced Nd_2O_3 nanoparticles.[26,27] These nanoparticles have great potential, further highlighted by their distinctive structural characteristics and their projected crystallite size of 24 nm using the Debye–Scherrer formula. Moreover, the Nd_2O_3 NP production process involves adding plant extract to increase crystallinity.[11] Wherein, bulk Nd_2O_3 NPs show bigger crystallite sizes and smaller pore sizes. The enhanced electron stream mitigation, refined crystalline characteristics, and greater charge separations driven by lattice strain are its unique properties, which make it possibly a dependable material with enormous potential for use in energy, optics, and catalysis.[28]

3.2. FTIR analysis

The functional groups present in the Nd_2O_3 NPs were characterized with FTIR spectroscopy over the spectrum range of 400 to 4000 cm^{-1}, as shown in Fig. 3. Great attention was paid

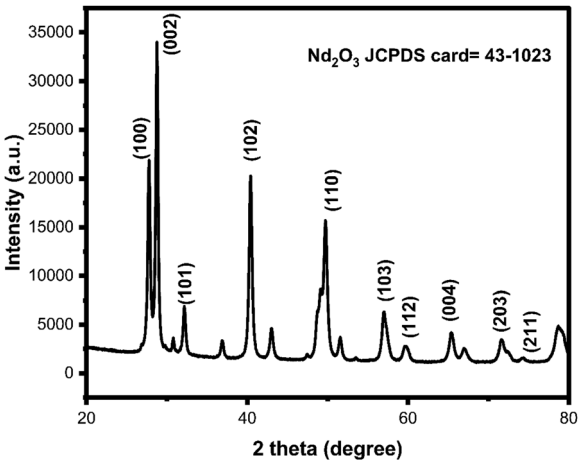

Fig. 2 XRD pattern of Nd_2O_3 nanoparticles synthesized using green methods with a *Caryota urens* leaf extract.

to the wide Nd–OH vibration peak at 3335 cm^{-1}, ascribed to water molecules absorbed on surface of the Nd_2O_3 NPs, making it more reasonable for oxygen–hydrogen (O–H) bond stretching vibrations.[29,30] An intense signal appeared at 2452 cm^{-1}, mainly due to the characteristic carbon atoms in the plant's bioactive compounds. The peaks showing at 1750 cm^{-1} and 1409 cm^{-1} were due to the surface chemistry and bonding configurations of Nd_2O_3 NPs, unveiling the interactions of primary amine and carbon compounds found in plant biomolecules.[31,32] The detailed interactions between NPs and bioactive compounds from the plants reveal their surface characteristics and chemical interactions. The conversion of Nd^{3+} ions into O^{2-} ions is prompted due to biochemical interaction with the Nd_2O_3 NPs. The vibrational peak that appeared at 1059 cm^{-1} is significant for nanomaterial formation and is known to be due to the asymmetric and bending vibrations of the Nd–O and Nd–O–Nd bonds.[33] The absorption band at 854 cm^{-1} corresponds to the surface characteristics and functional groups of Nd_2O_3 NPs.[34] A peak strongly depicted at 691 cm^{-1} enables an intense understanding of

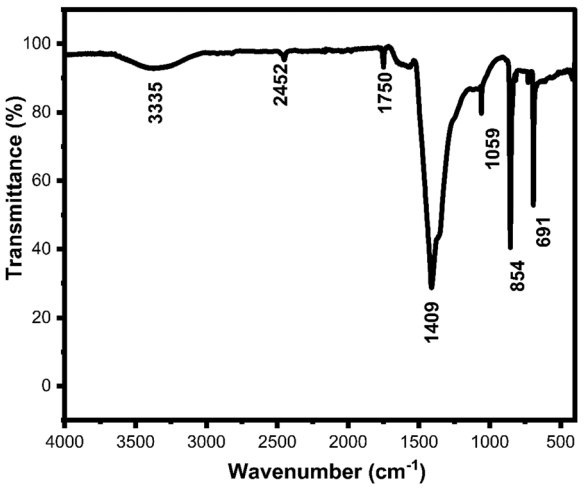

Fig. 3 FTIR spectrum of Nd_2O_3 nanoparticles.

composition and structural features of NPs. No new peaks have appeared in the FTIR spectrum, confirming remarkable purity of synthesized Nd_2O_3 NPs.[35]

3.3. Optical properties of Nd_2O_3 NPs

The optical properties of metal oxide constructions, specifically green-synthesized Nd_2O_3 NPs, were fully investigated using UV-DRS analysis, as shown in Fig. 4a, providing critical absorbance and bandgap spectrum information. The formation of these NPs, supported by a unique absorption edge around 210–280 nm in the UV-DRS spectra, involved reduction of Nd^{3+} ions and stabilization of O^{2-} ions. The absorption edge induced electron migration between energy bands, which resulted in significant color changes, with NPs exhibiting a pure milk-white color, confirming their effective synthesis.[36,37] For green-synthesized Nd_2O_3 NPs, the defect analysis using Kubelka–Munk relationships, as shown in Fig. 4b, produced a bandgap value of about 3.5 eV. The large bandgap makes it easier for charge carriers to migrate and separate efficiently on NP surfaces and improves the ability of those particles to reduce and oxidize.[38] The analysis provides insightful information about optical properties and defect features of NPs, potentially paving the way for their use in industries. To analyze the bandgap energy (E_g), DRS was performed in a UV-Vis spectrophotometer with a wavelength (λ) in the range of 200–800 nm, and bandgap energy was determined using equation[39]

$$F(R) \rightarrow \frac{(1-R_\infty)2}{R_\infty} \quad (5)$$

$$h\nu = \frac{1240}{\lambda} \quad (6)$$

$$R = \frac{1}{A} \quad (7)$$

where $F(R)$ is the Kubelka–Munk function, R_∞ is the reflectance (a.u.), $h\nu$ is the incident photon energy (eV), and λ is the wavelength associated with maximum absorbance (nm).

3.4. Chemical structure and morphology of Nd_2O_3 NPs

The green synthesis of Nd_2O_3 NPs is rigorously characterized in Fig. 5(a and b) and Fig. 6(a–c), revealing both structural properties using field emission scanning electron microscopy (FESEM) and energy-dispersive X-ray spectroscopy (EDX) mapping, respectively. The particles stand out for having two main shapes: elongated-spherical and conjoint spherical, which suggests a variety of morphologies on their surfaces (as shown in Fig. 5(a and b)). The presence of plant phytochemicals during the green production process directly contributed to this unique combination of shapes.[40,41] With a focus on Nd and O, Fig. 6(a) shows weight percentages and energy spectrum of the components within the NPs. Nd dominates composition, making up a substantially higher percentage than oxygen. This is further shown in Fig. 6(b), which shows unequivocally that the concentration of Nd atoms in green-mediated Nd_2O_3 NPs is three times higher than that of oxygen atoms. As shown in these NPs, the interaction of oxygen with metal components

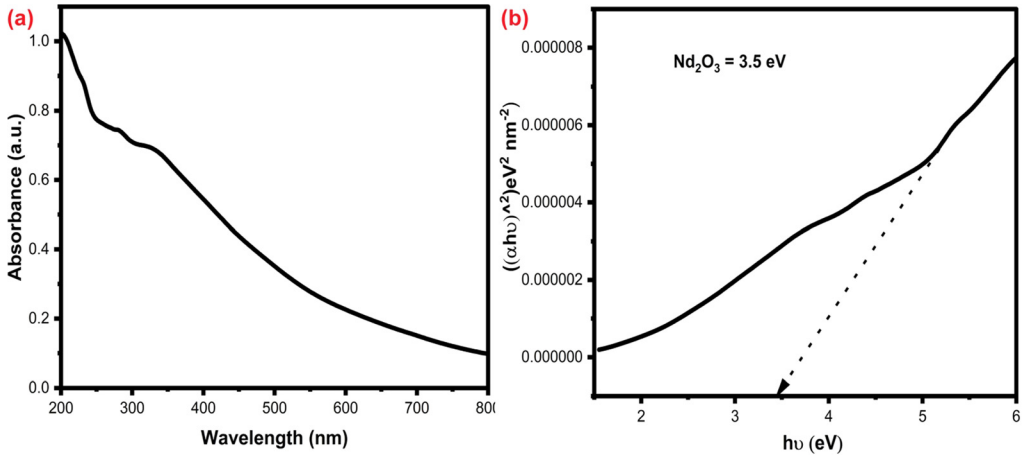

Fig. 4 UV-DRS (a) and bandgap (b) analysis of the Nd_2O_3 nanoparticles.

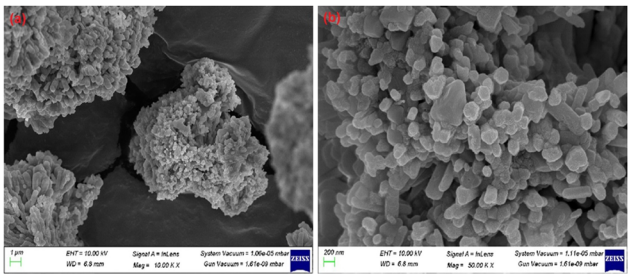

Fig. 5 FE-SEM images of the Nd_2O_3 nanoparticles at different magnifications of 10.00kx (a) and 50.00kx (b).

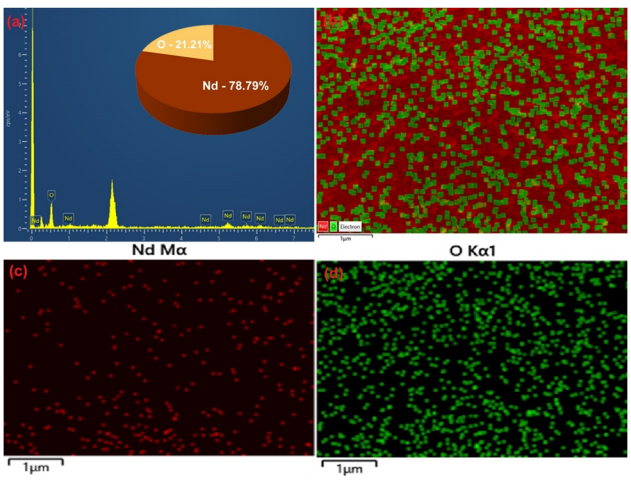

Fig. 6 EDX spectrum (c), elemental composition (d), and mapping of Nd_2O_3 nanoparticles (e)–(g) synthesized using a leaf extract of *Caryota urens*.

has a significant effect. It successfully reduces agglomeration and ultimately improves the particles' general stability. The processes, such as bacterial inactivation and disintegration, multiply the efficacy of the NPs due to the oxygen enhancement in the green production process, retaining the electron trapping. The composition comprises large Nd atoms with oxygen atoms and quasi-spherical forms of the NPs resulting from Nd_2O_3 NPs. The mapping results depicted in Fig. 6(a–c) confirm Nd and O distribution and spatial distribution of Nd and O enclosed in NPs is shown in Fig. 6a. Wherein, the neodymium and oxygen atoms hold one another and are scattered nearer and spectrum indicates the intriguing outcome of oxygen prevailing over neodymium in the NPs. This confirms the presence of a larger number of oxygen atoms than neodymium atoms in biosynthesized Nd_2O_3 NPs. Understanding the NPs' structural features and characteristics is important in knowing the physical distribution of neodymium and oxygen.

3.5. TEM analysis

TEM images of green-synthesized Nd_2O_3 NPs are shown in Fig. 7(a and b), unveiling morphological characteristics and particle size of synthesized Nd_2O_3 NPs in *C. urens* leaf extract. The TEM images show elongated and conjoint spherical morphology. The elongated spherical shape at a magnification of 100 nm resulted in evenly distributed polydisperse NPs. The obtained particles in range of 50 nm magnification level view show that particles are agglomerated in an elongated spherical shape. These agglomerations are formed in Nd_2O_3 NPs due to

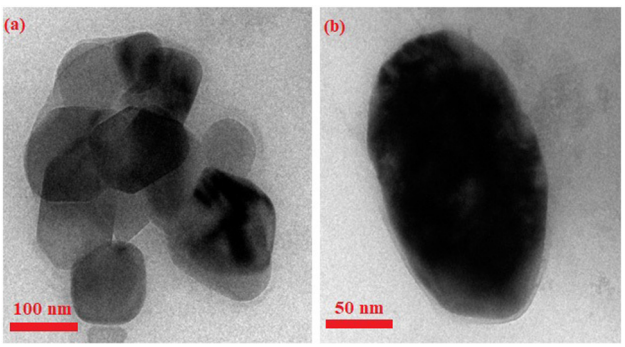

Fig. 7 TEM images of *Caryota urens* leaf extract-synthesized Nd_2O_3 nanoparticles.

biochemicals present in plants.[42,43] The X-ray diffraction (XRD) results are consistent with TEM results, wherein size of the NPs was found to be 25 nm. The broad bandgap associated with Nd_2O_3 NPs can be used to explain the polydisperse character of these biologically generated Nd_2O_3 NPs. The potential of these NPs for various applications, particularly in the context of materials science and advanced technologies, is highlighted by this thorough analysis of their morphology, size, and distribution. Therefore, Nd_2O_3 NPs in different mass proportions were confirmed by correlating the results of characterization techniques (XRD, FTIR, and SEM-EDX). The Nd_2O_3 NPs sample was used for photocatalytic heterogeneous application in pharmaceutical pollutants due to the narrow E_g (3.5 eV) and increased light absorption during the heterogeneous photocatalysis process.

4. Evaluation of photocatalytic activity

Fig. 8(a–d) shows the photocatalytic breakdown of TC caused by visible light using green-synthesized Nd_2O_3 NPs. Pharmaceutical pollutants can be more efficiently degraded by metal oxide-based photocatalysts. TC is prone to rapid degradation due to its interaction with high intensity light.[38–41] The two powerful benzene rings that make up the molecular structure of TC are essential for its ability to bind and form bonds with other chemical substances. Fig. 8 absorbance spectra, taken at 10-minute intervals, show that light gradually dissociates the binding of TC as it passes through the TC solution and Nd_2O_3 NPs. The Nd_2O_3 NPs made *via* green synthesis demonstrated good catalytic activity, degrading TC by 92% in under 40 minutes. This effectiveness could be due to the Nd_2O_3 NPs' broad bandgap, and capping effect of chemicals produced from plants, which regulate recombination processes and provide more host electrons that improve catalytic degradation. The photon energy is used for electrons' excitation in the valence band (VB) transition to the conduction band (CB). Defects are created in the VB during redox reactions. With breakdown of TC structure caused by this activity, superoxide (O^{2-}), and hydroxyl radicals (OH^-) are created. The increased surface area and active spots of Nd_2O_3 NPs also prevent TC molecules from attaching to them. TC is broken down into harmless CO_2 and H_2O molecules thanks to the produced free radicals and Nd_2O_3 NPs.

4.1. Possible photocatalytic mechanism

During the photocatalysis, following reactions take place:

Creation of electron–hole pairs upon visible light absorption by Nd_2O_3:

$$Nd_2O_3 + h\nu(\text{visible}) \rightarrow e^- + h^+ \quad (8)$$

TC molecules attach to the surfaces of Nd_2O_3 NPs.

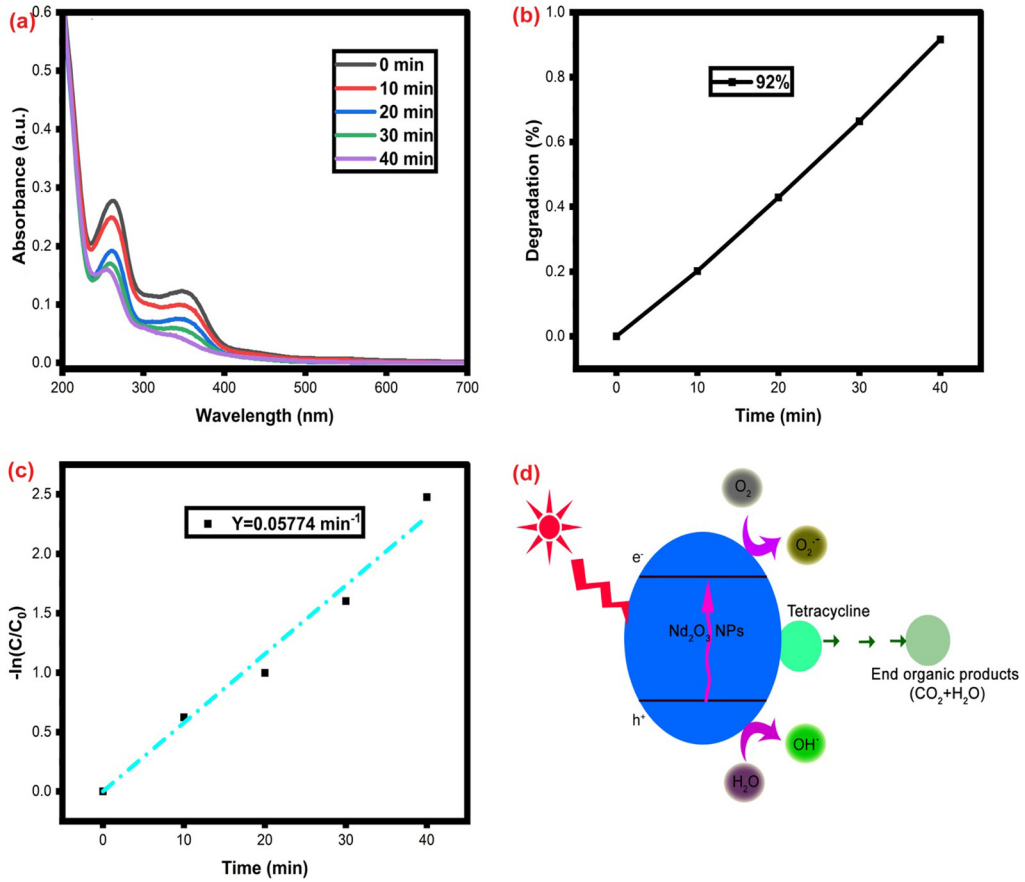

Fig. 8 Photocatalytic experiment of the Nd_2O_3 nanoparticles against tetracycline.

Table 1 Photocatalytic comparison table of different NPs with various antibiotics

Samples	Antibiotics	Molecular formula	Structure	Light	Time (min)	Degradation (%)	Ref.
WO_3/g-C_3N_4/h-BN	TC	$C_{22}H_{24}N_2O_8$	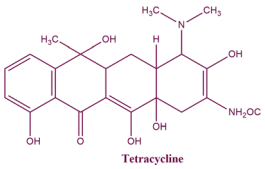 Tetracycline	Visible light	60	81.4	44
CuO–Cu_2O/GO	TC	$C_{22}H_{24}N_2O_8$	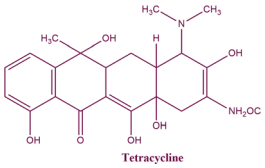 Tetracycline	Visible light	120	90	45
Fe_2O_3@PNH	TC	$C_{22}H_{24}N_2O_8$	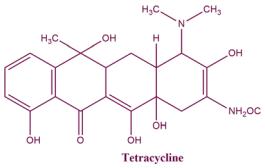 Tetracycline	Visible light	120	90	46
$BiVO_4$	Oxytetracycline	$C_{22}H_{24}N_2O_9$	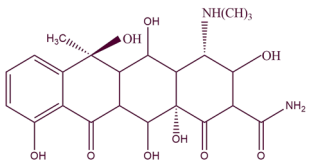	Visible	240	55	47
$BiVO_4$	Oxytetracycline	$C_{22}H_{24}N_2O_9$	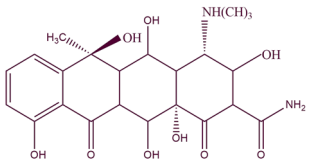	Solar	240	83	48
AgCl/$BiVO_4$	Oxytetracycline	$C_{22}H_{24}N_2O_9$	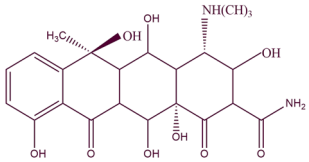	Visible	120	77	49
$BiVO_4$	TC	$C_{22}H_{24}N_2O_8$	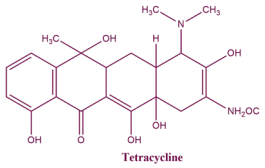 Tetracycline	Solar	240	72	50
Ti/$BiVO_4$	TC	$C_{22}H_{24}N_2O_8$	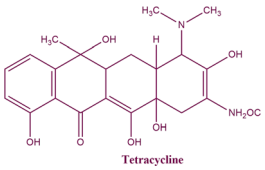 Tetracycline	Visible	180	60	51
g-C_3N_4/$BiVO_4$	TC	$C_{22}H_{24}N_2O_8$	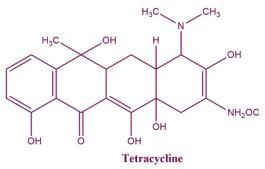 Tetracycline	Visible	60	60	52
H_2-$BiVO_4$	TC	$C_{22}H_{24}N_2O_8$	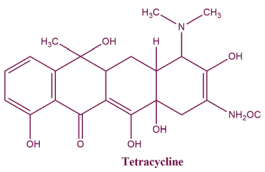 Tetracycline	Visible	240	75	53

Table 1 (*continued*)

Samples	Antibiotics	Molecular formula	Structure	Light	Time (min)	Degradation (%)	Ref.
$BiVO_4$/rGH-3	TC	$C_{22}H_{24}N_2O_8$	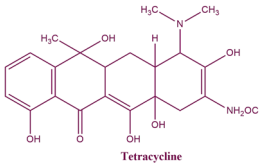 Tetracycline	Visible	120	73	54
$CuO/BiVO_4$	TC	$C_{22}H_{24}N_2O_8$	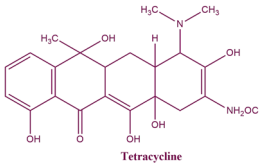 Tetracycline	Visible	50	28	55
$BiVO_4/TiO_2$	TC	$C_{22}H_{24}N_2O_8$	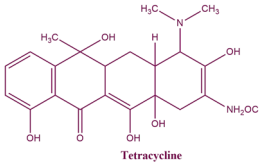 Tetracycline	Visible	60	73	56
Nd_2O_3	TC	$C_{22}H_{24}N_2O_8$	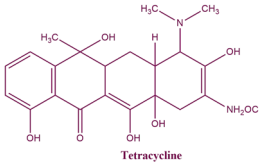 Tetracycline	Visible	40	92	[Present work]

$$TC + Nd_2O_3 \rightarrow TC\text{–}Nd_2O_3 \quad (9)$$

Electrons move from the CB of Nd_2O_3 to the TC molecules that are adsorbed on its surface.

$$e^-(Nd_2O_3) \rightarrow TC\text{–}Nd_2O_3 \quad (10)$$

The TC molecules adsorbed on Nd_2O_3 interact with the VB holes, and as a result, superoxide radicals formed.

$$h^+(Nd_2O_3) + TC\text{–}Nd_2O_3 \rightarrow TC + Nd_2O_3 + h^+ \quad (11)$$

$$O_2 + e^-(Nd_2O_3) \rightarrow O_2^{\bullet -} \quad (12)$$

$$O_2^{\bullet -} + h^+(Nd_2O_3) \rightarrow HO_2^{\bullet} \quad (13)$$

Continuous generation of superoxide and hydroxyl radicals through reactions with water molecules leads to the degradation of TC.

$$O_2 + e^-(Nd_2O_3) \rightarrow O_2^{\bullet -} \quad (14)$$

$$O_2^{\bullet -} \rightarrow HO_2 \rightarrow HO_2^{\bullet} + OH^- \quad (15)$$

$$2HO_2^{\bullet} \rightarrow H_2O_2 + O_2 \quad (16)$$

$$TC^{\bullet} + OH^- \rightarrow TC(H_2O + CO_2) \quad (17)$$

Under visible light irradiation, photocatalytic degradation of TC by Nd_2O_3 NPs involves several key steps: the generation of electron–hole pairs, adsorption of TC molecules onto the NP surfaces, transfer of electrons to these adsorbed molecules, and subsequent production of superoxide ($O_2^{\bullet -}$) and hydroxyl radicals (OH^-) through reactions with holes and water molecules. These reactive radicals ultimately lead to breakdown of TC into harmless byproducts. The degradation efficiency of Nd_2O_3 NPs, synthesized through environmentally friendly methods, was evaluated using pseudo-first-order kinetics. The graphical representation in Fig. 8 illustrates degradation rate constant, showcasing the photocatalytic performance and durability of these green-synthesized NPs in TC degradation. Table 1 compares photocatalytic efficiency of various antibiotic drugs using different NPs and light sources. Each entry in Table 1 presents a specific nanoparticle composition, targeted antibiotic, type of light employed, duration of exposure, and the resultant degradation efficiency. Prominent compositions include WO_3/g-C_3N_4/h-BN, CuO–Cu_2O/GO, and Fe_2O_3@PNH, each showcasing high degradation percentages of TC under visible light within 60 to 120 minutes. Moreover, different variants of $BiVO_4$ composites exhibited varying efficiencies, with pure $BiVO_4$ showing improved degradation under solar light compared to visible light. Conspicuously, the present work featuring Nd_2O_3 NPs displayed exceptional efficacy, achieving a remarkable 92% degradation of TC within a mere 40 minutes under visible light, surpassing the performance of all other tested photocatalysts. This superior performance can be attributed to Nd_2O_3's efficient light absorption, effective charge separation, and high reactivity, facilitating the rapid degradation of antibiotics.

Mechanistically, photocatalysis involves the generation of electron–hole pairs upon light absorption, followed by reactive oxygen species (ROS) that degrade the antibiotic molecules. Substantially, the electron–hole pair generation and ROS formation optimal bandgap are suitable for efficient visible light absorption and catalyst performance, prompted by metal oxides.[57] The increasing charge separation efficiency and the

additional active sites by encapsulating carbon-based materials such as graphene oxide (GO) and graphitic carbon nitride (g-C_3N_4) enhance photocatalytic activity.[58]

Composite materials, including Ag/$BiVO_4$ and $BiVO_4$/TiO_2, exhibit synergistic effects, combining the properties of metal oxides with those of other materials to enhance light absorption, charge separation, and surface area, resulting in improved photocatalytic efficiencies.[59] The Nd_2O_3 NPs remain important photocatalysts for breaking down many substances such as paracetamol, amoxicillin, ciprofloxacin, and TC. The study shows that Nd_2O_3 NPs degrade TC more effectively under visible light than under UV exposure. This is especially important because visible light is more energy-efficient and environmentally friendly than UV light. The current study also describes the environmentally friendly manufacture of highly crystalline Nd_2O_3 NPs using a plant extract and their superior photocatalytic activity for TC breakdown under visible light irradiation, achieving an efficiency of 92%.

5. Effect of Nd_2O_3 NPs on bacterial cultures

The antibacterial efficacy of Nd_2O_3 NPs was analyzed using bacterial cultures *i.e.*, *S. aureus* and *E. coli* Fig. 9(a and b). All the concentrations (25–100 μg mL^{-1}) of Nd_2O_3 NPs effectively inhibited the growth of both types of bacterial cells. However, increased growth inhibition was observed at 100 μg mL^{-1}, and least bacterial growth inhibition was noticed at 25 μg mL^{-1}. Therefore, this result, exhibited by increasing the Nd_2O_3 NP concentration from 25 μg mL^{-1} to 100 μg mL^{-1}, affects the bacterial growth. The control antibiotic exhibits remarkable antibacterial activity against both bacterial cultures. Similarly, Nd_2O_3 NPs prepared by the leaf extract of *Andrographis paniculata* exhibited excellent antibacterial activity against *E. coli* and *S. aureus* bacterial cultures.[55] Another report stated that Nd_2O_3 NPs synthesized by calcination process also showed antibacterial potential of NPs against various bacterial cultures, including *Micrococcus luteus*, *Staphylococcus aureus*, *Salmonella typhimurium*, and *Escherichia coli*.[60] Possibly, the bacterial cell proliferation was controlled by oxonium ions discharged from the Nd_2O_3 NPs.[61] Additionally, Nd_2O_3 NPs of reactive oxygen species might be involved in oxidative stress in bacterial cells.[62] This results in malfunction of cellular biomolecules and finally leads to the ruin of cells.

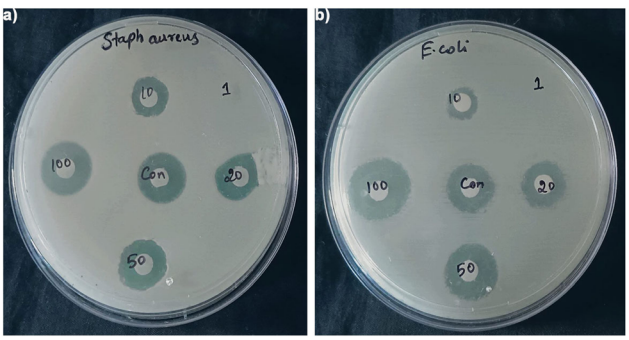

Fig. 9 Antibacterial activity of the Nd_2O_3 nanoparticles against *S. aureus* and *E. coli*.

6. Conclusion

In summary, a novel supramolecular assembly of green-mediated Nd_2O_3 NPs was assessed by their application in sustainability threats and biomedical applications. Further thermal treatment under a static air atmosphere changes the $Nd(NO_3)_3{\cdot}6H_2O$ with the O atom. The oxygen defects give Nd_2O_3 the highest stability, as confirmed by UV calculations. The resulting Nd_2O_3 photocatalyst demonstrates outstanding vis. light harvesting, charge carrier transition, and optical properties. In addition, it shows the highest electron density at the CB edge, which makes it a strong reduction photocatalyst. This result was further evidenced by more $^{\bullet}OH$ generation than in the control experiments. Furthermore, Nd_2O_3 NPs exhibited excellent photocatalytic performance in the degradation of TC under visible light irradiation within 40 min. The Nd_2O_3 NPs prepared by the *C. urens* plant extract showed their effective potency in the growth of bacterial cultures, *E. coli* and *S. aureus*. Therefore, Nd_2O_3 NPs emerge as promising candidates to meet the sustainable development goals.

The green-mediated synthesis of Nd_2O_3 NPs showed encouraging photocatalytic and antibacterial efficacy; nevertheless, many hurdles arose during the investigation. A significant challenge was attaining uniformity in NP morphology and size distribution due to the diversity in the phytochemical makeup among different leaf batches. Seasonal and geographical differences in plant bioactive components affected the reducing and stabilizing efficacy of the extract, hence influencing NP homogeneity. Moreover, regulating the aggregation of NPs was a problem, particularly during the drying and calcination phases, which might influence surface area and the availability of active sites. A third limitation was the limited tunability of the bandgap; although a bandgap of 3.5 eV was attained, additional optimization is required for improved visible-light absorption. Furthermore, although there are potential antibacterial effects, the precise molecular processes by which ROS formed by Nd_2O_3 disrupt bacterial cells remain inadequately elucidated and necessitate additional mechanistic investigations. Ultimately, enhancing the synthesis process for industrial applications is a difficult due to the necessity for meticulous regulation of green synthesis parameters and extract preparation conditions. Confronting these issues in forthcoming research will be essential for converting laboratory-scale discoveries into viable, scalable environmental and medicinal products.

Conflicts of interest

There are no conflicts to declare.

Data availability

The data that support the plots in this paper and other findings of this study are available from the corresponding author upon

reasonable request. Financial support: Funded by Next Generation EU for PRIN 2022 PNRR: M4.C2.1.1 "Progetti di Ricerca di Rilevante Interesse Nazionale (PRIN)" – Prot. P2022EWZFB – Unitised Regenerative Fuel Cell with Anion Exchange Membrane as Electrolyte (UNIRE), CUP B53D23025680001.

References

1 A. Javdani-Mallak and I. Salahshoori, Environmental pollutants and exosomes: A new paradigm in environmental health and disease, *Sci. Total Environ.*, 2024, 171774.
2 T. Li, *et al.*, A review of the influence of environmental pollutants microplastics, pesticides, antibiotics, air pollutants, viruses and bacteria on animal viruses, *J. Hazard. Mater.*, 2024, 133831.
3 S. Muzammal, *et al.*, Polymer-supported nanomaterials for photodegradation: Unraveling the methylene blue menace, *Energy Convers. Manage.:X*, 2024, 100547.
4 D. Wu, *et al.*, Persistence and potential risks of tetracyclines and their transformation products in two typical different animal manure composting treatments, *Environ. Pollut.*, 2024, **341**, 122904.
5 X. Zhang, *et al.*, Contamination distribution and non-biological removal pathways of typical tetracycline antibiotics in the environment: a review, *J. Hazard. Mater.*, 2024, **463**, 132862.
6 S. GokulaKrishnan, G. Arthanareeswaran and D. R. Devi, Bi_2WO_6 nanoparticles anchored on membrane by grafting via in-situ polymerization for the treatment of antibiotic and pesticides wastewater, *Chemosphere*, 2024, **351**, 141214.
7 M. Xie, *et al.*, Antibacterial nanomaterials: mechanisms, impacts on antimicrobial resistance and design principles, *Angew. Chem., Int. Ed.*, 2023, **62**(17), e202217345.
8 B. A. Taha, *et al.*, Synergizing Nanomaterials and Artificial Intelligence in Advanced Optical Biosensors for Precision Antimicrobial Resistance Diagnosis, *ACS Synth. Biol.*, 2024, **13**, 1600–1620.
9 Z. H. Jabbar, *et al.*, The latest progress in the design and application of semiconductor photocatalysis systems for degradation of environmental pollutants in wastewater: Mechanism insight and theoretical calculations, *Mater. Sci. Semicond. Process.*, 2024, **173**, 108153.
10 A. Verma and Y.-P. Fu, The prospect of CuxO-based catalysts in photocatalysis: From pollutant degradation, CO_2 reduction, and H_2 production to N_2 fixation, *Environ. Res.*, 2024, **241**, 117656.
11 T. Munawar, *et al.*, Novel direct dual-Z-scheme ZnO-Er_2O_3-Nd_2O_3@ reduced graphene oxide heterostructured nanocomposite: synthesis, characterization and superior antibacterial and photocatalytic activity, *Mater. Chem. Phys.*, 2020, **253**, 123249.
12 P. Arul, *et al.*, Enhancing the energy storage performance of titanium dioxide electrode material by green doping of Nd_2O_3 nanoparticles for electrochemical supercapacitors, *J. Indian Chem. Soc.*, 2024, **101**(7), 101177.
13 M. Arghavan, A. Sabouri-Dodaran and M. S. Ghamsari, Efficient route for preparation of Nd^{3+} doped Y_2O_3 nanoparticles at intermediate temperature, *Heliyon*, 2024, **10**(4), 25864.
14 A. Zaki, *et al.*, *Synthesis, Characterization, and Optical Properties of Chitosan-Nd2O3 Nanocomposites*, 2024.
15 A. Abouhaswa and T. A. M. Taha, Synthesis, optical and magnetic properties of Nd_2O_3/borate strontium fluoride glasses, *Ceram. Int.*, 2024, **50**(7), 11032–11039.
16 H. Jayasimha, *et al.*, Green synthesis of CuO nanoparticles: A promising material for photocatalysis and electrochemical sensor, *Sens. Int.*, 2024, **5**, 100254.
17 M. A. Albo Hay Allah and H. A. Alshamsi, Green synthesis of ZnO NPs using Pontederia crassipes leaf extract: characterization, their adsorption behavior and anti-cancer property, *Biomass Convers. Biorefin.*, 2024, **14**(9), 10487–10500.
18 B. Dülger, *et al.*, Green synthesis of TiO_2 nanoparticles using Aloe Vera extract as catalyst support material and studies of their catalytic activity in dehydrogenation of Ethylenediamine Bisborane, *Int. J. Hydrogen Energy*, 2024, **75**, 466–474.
19 A. Ranawake and R. Pathirana, Indigenous knowledge in the Kithul (Caryota urens L.) industry of Sri Lanka and its scientific basis, *Genet. Resour. Crop Evol.*, 2024, 1–20.
20 S. A. Abd Elmohsen, *et al.*, Photocatalytic degradation of biological contaminant (E. coli) in drinking water under direct natural sunlight irradiation using incorporation of green synthesized TiO_2, Fe_2O_3 nanoparticles, *Biomass Convers. Biorefin.*, 2024, 1–22.
21 R. W. Ranaweera, *et al.*, Synthesis of nano zero valent zinc-reduced graphene oxide nanocomposite using a novel electrochemical technique for the adsorptive degradation of methyl orange, *Colloids Surf., A*, 2024, **703**, 135250.
22 T. Sathish, *et al.*, Sustainable nanoparticles of Non-Zero-valent iron (nZVI) production from various biological wastes, *J. King Saud Univ., Sci.*, 2024, 103553.
23 R. Han, *et al.*, One-step self-assembled ZIF-derived flower-like carbon enhances reactivity of zero-valent iron during persulfate activation, *Sep. Purif. Technol.*, 2025, **356**, 129844.
24 Q. Li, *et al.*, Selective Tl (I) Removal by Prussian Blue–Zero Valent Iron Nanoparticles, *ACS Appl. Nano Mater.*, 2024, **7**, 24368–24376.
25 D. F. Ollis, Kinetics of photocatalyzed reactions: five lessons learned, *Front. Chem.*, 2018, **6**, 378.
26 D. A. Ananth, *et al.*, Chemical constituents, in vitro antioxidant and antimicrobial potential of Caryota urens L, *Free Radicals Antioxid.*, 2013, **3**(2), 107–112.
27 S. Ke, Y. Wang and Z. Pan, Effects of precipitant and surfactant on co-precipitation synthesis of $Nd_2Si_2O_7$ ceramic pigment, *Dyes Pigm.*, 2015, **118**, 145–151.
28 S. Bhaskar and S. S. Ramamurthy, Mobile phone-based picomolar detection of tannic acid on Nd_2O_3 nanorod–metal thin-film interfaces, *ACS Appl. Nano Mater.*, 2019, **2**(7), 4613–4625.
29 M. Lembang, *et al.*, A facile method for green synthesis of Nd_2O_3 nanoparticles using aqueous extract of Terminalia catappa leaf, *AIP Conf. Proc.*, 2018, 020093.

30 D. Zhao, *et al.*, Influence of a Reduction Process on the Phase Component and Magnetic Properties of NdFeB Magnetic Nanoparticles, *J. Nanosci. Nanotechnol.*, 2021, **21**(1), 715–719.
31 M. Sundrarajan and V. Muthulakshmi, Green synthesis of ionic liquid mediated neodymium oxide nanoparticles by Andrographis paniculata leaves extract for effective biomedical applications, *J. Environ. Chem. Eng.*, 2021, **9**(1), 104716.
32 V. Muthulakshmi, C. Dhilip Kumar and M. Sundrarajan, Green synthesis of ionic liquid mediated neodymium oxide nanoparticles via Couroupita guianensis abul leaves extract with its biological applications, *J. Biomater. Sci., Polym. Ed.*, 2022, **33**(8), 1063–1082.
33 S. Maroufi, R. Khayyam Nekouei and V. Sahajwalla, A green route to synthesize Pr^{3+}/Dy^{3+}-doped Nd_2O_3 nanoreplicas from Nd–Fe–B magnets, *ACS Sustainable Chem. Eng.*, 2018, **6**(3), 3402–3410.
34 S. Zinatloo-Ajabshir, S. Mortazavi-Derazkola and M. Salavati-Niasari, Sonochemical synthesis, characterization and photodegradation of organic pollutant over Nd_2O_3 nanostructures prepared via a new simple route, *Sep. Purif. Technol.*, 2017, **178**, 138–146.
35 I. Selmi and B. Ouertani, Characterization of Nd_2O_3/Psi Interface, Obtained by Doping Porous Silicon with Rare Earth Oxide, Nd_2O_3.
36 A. A. Ahmed, *et al.*, Neodymium oxide nanoparticles synthesis using phytochemicals of leaf extracts of different plants as reducing and capping agents: Growth mechanism, optical, structural and catalytic properties, *J. Chin. Chem. Soc.*, 2022, **69**(3), 462–475.
37 K. Bahram and M. Maryam, Synthesis and characterization of Nd_2O_3 nanoparticles using urea as precipitation agent, *J. Transition Met. Complexes*, 2023, 246148.
38 B. Umesh, *et al.*, Synthesis and characterization of spherical and rod like nanocrystalline Nd_2O_3 phosphors, *J. Alloys Compd.*, 2011, **509**(4), 1146–1151.
39 E. S. Welter, *et al.*, Methodological investigation of the band gap determination of solid semiconductors via UV/Vis spectroscopy, *ChemPhotoChem*, 2023, **7**(6), e202300001.
40 M. Mohammadi, B. Khoshnevisan and M. Moradian, Synthesis and Characterization of Nd_2O_3 Nanoparticles Using Urea As Precipitation Agent, *J. Transition Met. Complexes*, 2023, 246148.
41 S. Vijayaram, *et al.*, Applications of green synthesized metal nanoparticles—a review, *Biol. Trace Elem. Res.*, 2024, **202**(1), 360–386.
42 R. Bouhajeb, *et al.*, Green Synthesis of Highly Monodisperse and Spherical Ag Nanoparticles by a Combination of Teucrium ramosissimum Desf.(Lamiaceae) Extracts with Emphasis on the Stabilizing and Capping Biomolecules, *ACS Sustainable Chem. Eng.*, 2024, **12**(10), 4132–4145.
43 S. Mohanaparameswari, *et al.*, Green Synthesis of Silver Oxide Nanoparticles Using Plectranthus amboinicus and Solanum trilobatum Extracts as an Eco-friendly Approach: Characterization and Antibacterial Properties, *J. Inorg. Organomet. Polym. Mater.*, 2024, 1–21.
44 Y. Yang, *et al.*, The synthesis of h-BN-modified Z-scheme WO_3/g-C_3N_4 heterojunctions for enhancing visible light photocatalytic degradation of tetracycline pollutants, *ACS Omega*, 2022, **7**(7), 6035–6045.
45 Z. Zhang, *et al.*, Facile hydrothermal synthesis of CuO–Cu_2O/GO nanocomposites for the photocatalytic degradation of organic dye and tetracycline pollutants, *New J. Chem.*, 2020, **44**(16), 6420–6427.
46 T. Zhang, *et al.*, Polymer-coated Fe_2O_3 nanoparticles for photocatalytic degradation of organic materials and antibiotics in water, *ACS Appl. Nano Mater.*, 2020, **3**(9), 9200–9208.
47 T. Senasu, *et al.*, Sunlight-driven photodegradation of oxytetracycline antibiotic by $BiVO_4$ photocatalyst, *J. Solid State Chem.*, 2021, **297**, 122088.
48 C. Ma, *et al.*, $BiVO_4$ ternary photocatalyst co-modified with N-doped graphene nanodots and Ag nanoparticles for improved photocatalytic oxidation: A significant enhancement in photoinduced carrier separation and broad-spectrum light absorption, *Sep. Purif. Technol.*, 2021, **264**, 118423.
49 Y. Dai, *et al.*, High photocatalytic degradation efficiency of oxytetracycline hydrochloride over Ag/AgCl/$BiVO_4$ plasmonic photocatalyst, *Solid State Sci.*, 2019, **96**, 105946.
50 K. Hemavibool, T. Sansenya and S. Nanan, Enhanced photocatalytic degradation of tetracycline and oxytetracycline antibiotics by $BiVO_4$ photocatalyst under visible light and solar light irradiation, *Antibiotics*, 2022, **11**(6), 761.
51 N. T. K. Huyen, *et al.*, Fabrication of titanium doped $BiVO_4$ as a novel visible light driven photocatalyst for degradation of residual tetracycline pollutant, *Ceram. Int.*, 2021, **47**(24), 34253–34259.
52 J. Kang, *et al.*, The enhanced peroxymonosulfate-assisted photocatalytic degradation of tetracycline under visible light by g-C_3N_4/Na-$BiVO_4$ heterojunction catalyst and its mechanism, *J. Environ. Chem. Eng.*, 2021, **9**(4), 105524.
53 C. Yang, *et al.*, Photocatalytic enhancement mechanism insight for $BiVO_4$ induced by plasma treatment under different atmospheres, *J. Alloys Compd.*, 2022, **890**, 161883.
54 C. Ma, *et al.*, Construction of quantum dots self-decorated $BiVO_4$/reduced graphene hydrogel composite photocatalyst with improved photocatalytic performance for antibiotics degradation, *Chemosphere*, 2021, **275**, 130052.
55 X. Chen, *et al.*, Degradation of tetracycline hydrochloride by coupling of photocatalysis and peroxymonosulfate oxidation processes using CuO-$BiVO_4$ heterogeneous catalyst, *Process Saf. Environ. Prot.*, 2021, **145**, 364–377.
56 W. Wang, *et al.*, Enhanced photocatalytic degradation performance of organic contaminants by heterojunction photocatalyst $BiVO_4$/TiO_2/RGO and its compatibility on four different tetracycline antibiotics, *Adv. Powder Technol.*, 2019, **30**(9), 1882–1896.
57 M. T. Elabbasy, *et al.*, Adsorption and bacterial performance of Nd_2O_3 modified Ag nanoparticles with enhanced degradation of methylene blue, *Sci. Rep.*, 2024, **14**(1), 9877.
58 K. Alshammari, Influence of ZrO_2 nanoparticles on the structural and photocatalytic properties of three-dimensional PVA/g-C_3N_4 polymer films, *J. Alloys Compd.*, 2024, **1003**, 175622.

59 B. Patial, *et al.*, $BiVO_4$-based heterojunction nanophotocatalysts for water splitting and organic pollutant degradation: a comprehensive review of photocatalytic innovation, *Rev. Inorg. Chem.*, 2024, **44**, 495–519.
60 M. S. Al-Fakeh and N. F. Al-Otaibi, Nd_2O_3, Cr_2O_3, and V_2O_3 nanoparticles via calcination: Synthesis, characterization, antimicrobial and antioxidant activities, *J. Nanotechnol.*, 2022, **2022**(1), 7794939.
61 S. Bhaskar, V. Srinivasan and S. S. Ramamurthy, Nd_2O_3-Ag nanostructures for plasmonic biosensing, antimicrobial, and anticancer applications, *ACS Appl. Nano Mater.*, 2023, **6**(2), 1129–1145.
62 K. Gopinath, *et al.*, Fabrication of neodymium (Nd), cadmium (Cd) and Nd: Cd doped hybrid copper oxide nanocomposites: evaluation of their antibacterial activity and cytotoxicity against human L132 cell line, *Ceram. Int.*, 2023, **49**(18), 29933–29947.